Processing and Application of Ceramics 14 [1] (2020) 32–39
https://doi.org/10.2298/PAC2001032F

Fabrication and properties of Si_2N_2O ceramics for microwave sintering furnace

Bingbing Fan[1], Wei Li[1], Fan Zhang[1,3], Hongxia Li[1,2], Rui Zhang[1,4], Guoqi Liu[2], Fan Qian[2,*], Yongqiang Chen[1,2,*]

[1]*School of Materials Science and Engineering, Zhengzhou University, Zhengzhou 450001, China*
[2]*Sinosteel Luoyang Institute of Refractories Research Co., Ltd., Henan 471039, China*
[3]*Henan Vocational College of Information and Statistics, Zhengzhou 450008, China*
[4]*Zhengzhou Institute of Aeronautical Industry Management, Henan 450015, China*

Received 3 September 2019; Received in revised form 26 November 2019; Accepted 28 January 2020

Abstract

The Si_2N_2O ceramics with low dielectric constant, low thermal diffusivity and high thermal shock resistance were successfully prepared by vacuum sintering. The amorphous Si_3N_4 was used as raw material with Li_2CO_3 as sintering additive. The phase, microstructure, oxidized resistance, mechanical and dielectric properties of the Si_2N_2O ceramics were investigated. XRD analysis showed that the suitable content of Li_2CO_3 could promote the generation of Si_2N_2O ceramics. However, the excess or insufficient amount of Li_2CO_3 additive would cause decomposition of Si_2N_2O phase. The Li_2O volatilized at high temperature leaving highly pure (99.63%) porous Si_2N_2O ceramics. The flexural strength of the porous Si_2N_2O ceramics (with ≈49.19% of open porosity) was about 30 MPa, the residual strength ratio was more than 70% after 1300 °C quenching in air. The SiO_2 layer formed by oxidization could prevent Si_2N_2O ceramics from further oxidizing. Therefore, these Si_2N_2O ceramics will be excellent thermal insulation and wave-transparent materials for high temperature microwave sintering furnace.

Keywords: *porous Si_2N_2O, Li_2CO_3 additive, vacuum sintering, dielectric properties, thermal shock resistance*

I. Introduction

As an advanced sintering technology, microwave sintering plays a key role in the field of ceramics fabrication and it has attracted considerable attention in recent years [1–4]. However, the lack of insulation and microwave transparent materials with excellent thermal shock resistance and dielectric properties limits the high temperature (>1300 °C) application [5]. Therefore, it is necessary to develop thermal insulation and wave-transparent materials for high temperature application in microwave sintering technique. So far, there are several high performance wave-transparent materials, such as β-SiAlON ceramics [6–8], Si_3N_4 ceramics [9–11], SiO_2 ceramics [12,13], Si_2N_2O ceramics [14–16] and related composite materials [17–20]. Among them, the Si_2N_2O ceramics is the only compound in the SiO_2-Si_3N_4 system and it has the lowest dielectric constant (6.0). The dielectric constants of β-SiAlON and Si_3N_4 are 8.8 and 7.9, respectively [8,21]. In addition, the Si_2N_2O ceramics possesses relatively low theoretical density (2.81 g/cm^3), high hardness (17–22 GPa), low thermal expansion coefficient (3.5×10^{-6} K^{-1}), high thermal stability up to 1750 °C and oxidation resistance, making it an ideal choice for thermal insulation and wave-transparent materials [8,14,21–24]. Many studies reveal that pure and dense Si_2N_2O ceramics exhibit excellent mechanical and dielectric properties, making it suitable for use in the wave-transparent field, such as the microwave sintering and missile radomes [20,21,25]. However, the sintered dense materials show poor thermal shock resistance (critical temperature difference of about 600 °C) and higher dielectric constant (6.17 at 1 MHz) [21,26], which is still too high for microwave sintering. Therefore, appropriate methods should be tested to improve thermal shock resistance and reduce

* Corresponding author: tel: +86 0379 64206330,
e-mail: *15294628626@163.com* (Yongqiang Chen)
e-mail: *afan@qq.com* (Fan Qian)

the dielectric constant. Many researchers have reported that porous ceramics possess both better thermal shock resistance and lower dielectric constant due to the lower air dielectric constant (1.0) [9,15]. Thus, the lower dielectric constant and better thermal shock resistance of porous Si_2N_2O ceramics could satisfy the requirements of the microwave sintering furnace.

Various processing techniques have been developed to prepare porous Si_2N_2O ceramics, such as gel-casting [27,28], adding pore former [15,29,30], and polymer-derived ceramics [31]. However, the impurities were left due to the incomplete reaction with each other, which seriously affected dielectric properties of materials. Recently, some reports utilized the characterization of rapid volatilization of Li_2O sintering additives at high temperature to reduce sintering additives residues [32–34], which might be beneficial for the fabrication of the pure porous Si_2N_2O ceramics.

In this paper, the Li_2CO_3 was used as precursor additive to form Li_2O at high temperature. By vacuum sintering, the Li_2O was discharged from porous Si_2N_2O ceramics. The influence of Li_2O content on the phase, morphology, mechanical and dielectric properties of Si_2N_2O ceramics was investigated. The effects of porosity and oxidation on dielectric properties were also discussed.

II. Experimental details

2.1. Materials preparation

Nano-sized amorphous Si_3N_4 powder (>99% purity, ~20 nm, Shanghai Chao Wei Nanotechnology Co., Ltd, China) was used as starting material (Fig. 1). It can be seen that the raw powder has homogeneous distribution and the average size of Si_3N_4 particles is about 50 nm. Li_2CO_3 (99% purity, Xilong Scientific Co., Ltd. China) in different amount (1.0, 2.0, 3.0 and 5.0 wt.%) was added to the amorphous Si_3N_4 powder as sintering additive. Si_3N_4 powders were attrition milled with different sintering additive content (1.0, 2.0, 3.0 and 5.0 wt.%) using PyNN, SPEX-8000M. The mixed powders were ultrasonically dispersed in ethanol for 15 min and then mixed by high energy milling for 1 h using a 375 ml Si_3N_4 bottle with Si_3N_4 balls.

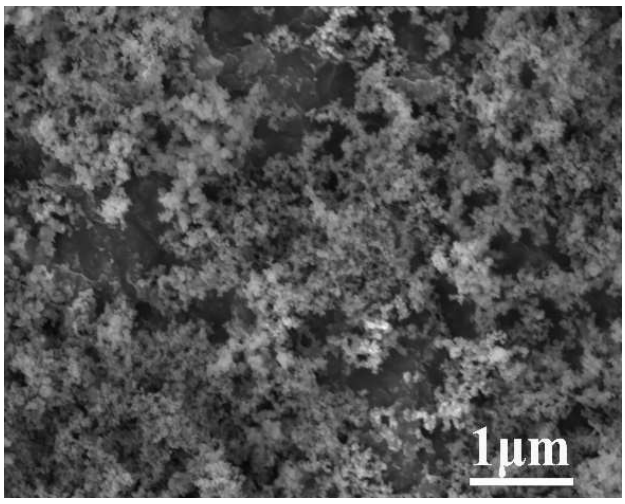

Figure 1. SEM micrograph of Si_3N_4 raw material

In order to increase oxygen content in the raw materials, the amorphous Si_3N_4 powder was pre-oxidized at 1000 °C for 2 h. The pre-oxidized amorphous Si_3N_4 powder and different content of the sintering additive were mixed and milled by Si_3N_4 balls media in ethanol for 30 min. Then, the mixtures were dried at 100 °C for 8 h under vacuum. The mixtures were sieved though a 100 mesh screen, then the powder mixtures were uniaxially pressed under 50 MPa to form rectangular green body (6 mm × 9 mm × 36 mm). The green pellets were placed in an alumina crucible and sintered in vacuum furnace with packing of Si_3N_4 powder by a multi-step sintering approach. Firstly, sintering temperature was increased to 1000 °C with the heating rate of 8 °C/min, then increased to 1450 °C with the heating rate of 5 °C/min. Secondly, the temperature was further increased to 1650 °C with the heating rate of 2 °C/min and held for 2 h, followed by natural cooling to room temperature.

The porosity was measured by the Archimedes displacement method. Three-point bending strength was determined at room temperature using a universal testing machine at a crosshead speed of 0.5 mm/min with a span of 30 mm. Fracture toughness (K_{IC}) was performed using the single-edge notched beam (SENB) method, the size of specimens was 3 mm × 4 mm × 20 mm with a notch of 2 mm depth and 0.2 mm width and a 16 mm span. The fracture toughness was calculated using the following equation:

$$K_{IC} = \frac{3PL\sqrt{a}}{2bh^2}\left[1.93 - 3.07\frac{a}{h} + 14.53\left(\frac{a}{h}\right)^2 - 25.07\left(\frac{a}{h}\right)^3 + 25.08\left(\frac{a}{h}\right)^4\right] \quad (1)$$

where P is the applied indentation load, L is the span, a is the specimen pre-crack depth, b is the sample cross section width and h is the sample cross section height [35].

Thermal shock resistance experiments were carried out in a muffle furnace at temperatures between 900 and 1300 °C in air. After the furnace was heated to the desired temperature, the ground and polished rectangular bars were put into the furnace and kept for 20 min. Then the samples were quenched in air and the residual flexural strength was performed using a universal testing machine. Five samples were characterized to get each final average value. The mass change was measured to evaluate Li content and the oxidation degree.

The microstructures were characterized by scanning electron microscopy (SEM, JEOL JSM-6700F, Japan). The phase was identified by X-ray diffraction (XRD, Beijing Purkinje General Instrument Co. Ltd, Cu-Kα radiation). The quantitative analysis of Si_2N_2O, Si_3N_4 and

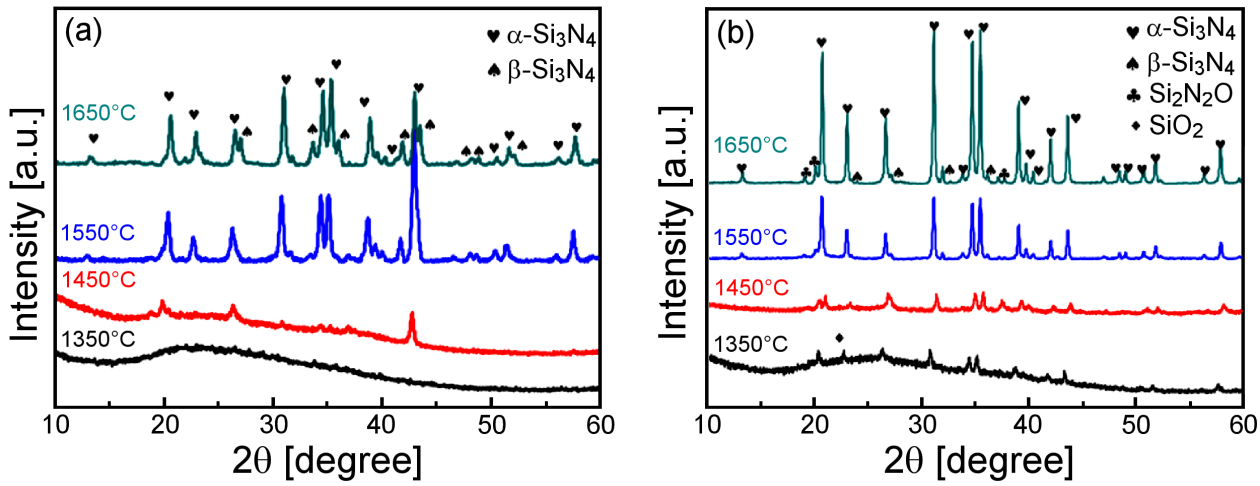

Figure 2. XRD patterns of amorphous Si_3N_4 powder (un-oxidized (a) and pre-oxidized (b)) heat treated at different temperatures

SiO_2 was calculated based on the peak intensity using the following equation:

$$X_i = \left(\frac{k_i}{I_i} \sum_{i=1}^{n} \frac{I_i}{k_i} \right)^{-1} \tag{2}$$

where k is the internal standard and I_i is the strongest peak's integrated intensity [36,37].

The residual contents of Li in the as-prepared samples after sintering were determined by inductively coupled plasma-atomic emission spectrometry (ICP-AES, Thermo Electron Corporation, MA). The samples were crushed into powders and ultrasonically etched in HNO_3/HF solution for 12 h to ensure complete dissolution of the Li in the liquid. The dielectric constant (ε) and loss tangent ($\tan\delta$) of the Si_2N_2O ceramics were measured on the Agilent N5244A vector network analyser system in the frequency range of 2–18 GHz at room temperature.

III. Results and discussion

3.1. Phase and microstructure

In order to study the influence of oxygen content on the crystallized product of amorphous Si_3N_4, the amorphous Si_3N_4 raw material was pre-oxidized in the muffle furnace in air at 1000 °C and the heating rate was 10 °C/min with 2 h holding. Comparison of the un-oxidized and pre-oxidized samples is shown in Fig. 2. It can be seen that amorphous Si_3N_4 is more crystallized at the same temperature after pre-oxidation. On the other hand, the Si_2N_2O and SiO_2 peaks appeared when the amorphous Si_3N_4 was oxidized, which proved that per-oxidation can provide a lot of oxygen and produces Si_2N_2O.

Figure 3 shows the phase evolution of the sintered bodies with 0, 1, 2, 3 and 5 wt.% of sintering additives after sintering at 1650 °C for 2 h. It can be seen from Fig. 3, that the sintered sample without any additives

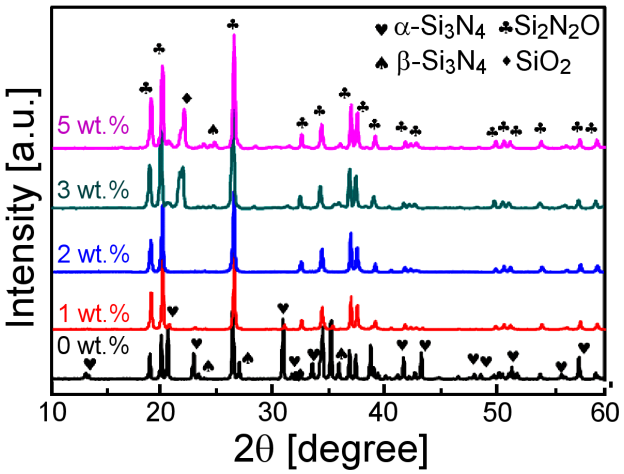

Figure 3. XRD patterns of the Si_2N_2O ceramics with different additive content sintered at 1650 °C for 2 h

consisted of α-Si_3N_4, Si_2N_2O and β-Si_3N_4. The residual Li content in the as-prepared samples has been detected by inductively coupled plasma-atomic emission spectrometry (ICP-AES, Thermo Electron Corporation, MA). The residual Li content decreased from 0.022% to 0.015% with the decrease of additive content from 5 to 1 wt.%.

The α-Si_3N_4 was the major phase, while Si_2N_2O and β-Si_3N_4 could also be detected. The single phase Si_2N_2O was prepared when the additive content was 2 wt.%. The α-Si_3N_4 peaks of the sample with 1 wt.% additive content can be observed in Fig. 3. This phenomenon indicates that the conversion of α-Si_3N_4 to Si_2N_2O was not complete due to the relatively low Li_2O liquid amount. The β-Si_3N_4 and SiO_2 peaks appeared when the additive content was higher than 3 wt.%, which proved that the decomposition of Si_2N_2O took place. In addition, the peaks of β-Si_3N_4 and SiO_2 were enhanced with the increasing of additive content as seen in Fig. 3. These results suggested that the decomposition of Si_2N_2O was easier in the rich Li_2O liquid envi-

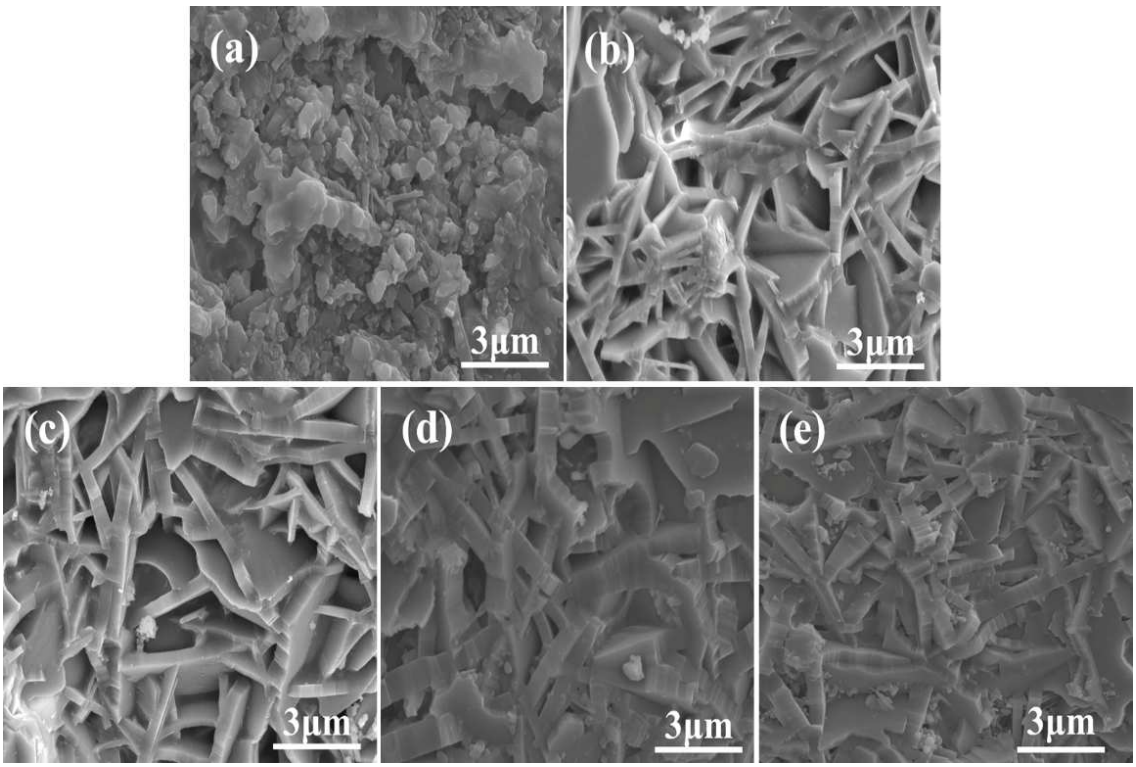

Figure 4. SEM morphology of the Si_2N_2O ceramics sintered at 1650 °C for 2 h with different Li_2O contents: a) 0, b) 1, c) 2, d) 3 and e) 5 wt.%

ronment. The decomposition reaction of Si_2N_2O mainly included the following equations [14,24]:

$$3\,Si_2N_2O(s) \longrightarrow 2\,Si_3N_4(s) + 3\,SiO(g) + N_2(g) \quad (3)$$

$$2\,Si_2N_2O(s) + 3\,O_2(s) \longrightarrow 4\,SiO(g) + 2\,N_2(g) \quad (4)$$

Figure 4 shows the typical morphology of the porous Si_2N_2O ceramics with different additive content after sintering at 1650 °C for 2 h. As shown in the Fig. 4a, small rod-shaped grains were present in the porous Si_2N_2O ceramics. Furthermore, it can be seen from Fig3. 4b-e that the samples with different Li_2O content exhibited a rod-shaped grain morphology. However, when the additive content was 3 wt.% or 5 wt.%, the typical elongated β-Si_3N_4 grains were visible as shown in Figs. 4d,e. According to the previous XRD analysis, the elongated β-Si_3N_4 grains came from the decomposition of Si_2N_2O. Granular morphology with a short grown rod-shaped crystal phase was present in Si_2N_2O ceramics when the additive content was 1 wt.% and the average size of α-Si_3N_4 was about 1 μm. However, typical elongated and needle-like β-Si_3N_4 grains were visible when the additive content was 5 wt.% and the average size of β-Si_3N_4 was about 2.5 μm.

The porosity and density of samples are listed in Table 1. The open porosity has been slightly decreased when the additive content was more than 2 wt.%. According to mass loss, three reasons were responsible for the porosity and mass loss: i) the decomposition of Si_2N_2O, ii) the decomposition of Li_2CO_3 and iii) the Li_2O evaporated when the vapour pressure of Li_2O was higher than 5 Pa at 1650 °C. The decomposition of Li_2CO_3 and evaporation of Li_2O lead to porosity increasing. So, the porosity decreasing indicates that the decomposition of Si_2N_2O can decrease porosity. In the Table 1, quantitative analysis showed that the fraction of Si_2N_2O reached minimum when the amount of additive content was 5 wt.%. This result is consistent with XRD patterns in Fig. 3. It was reported in literature [8,24,32] that the atomic diffusion became easier when the Si_2N_2O crystals were wetted by a low viscous melt of LiO_2-SiO_2. So the viscosity of the melts reduced with the increase of additive content, which facilitated the decomposition of Si_2N_2O.

Table 1. Porosity, density, mass loss and Si_2N_2O content of the specimens with different additive content

Additive content [wt.%]	Open porosity [%]	Density [g·cm^{-3}]	Mass loss [%]	Fraction of Si_2N_2O [%]
0	57.11	1.12	1.60	37.90
1	52.16	1.23	5.89	85.56
2	49.19	1.34	8.71	99.63
3	47.43	1.41	10.66	83.83
5	45.82	1.51	15.47	71.07

Table 2. Mechanical properties of the obtained samples with different additive content

Additive content [wt.%]	Bending strength [MPa]	Elastic modulus [GPa]	Fracture toughness [MPa·m$^{1/2}$]
1	18 ± 5.1	8.16 ± 1.5	1.12 ± 0.05
2	30 ± 4.7	13.7 ± 2.6	1.19 ± 0.08
3	44 ± 6.6	19.4 ± 2.2	1.34 ± 0.06
5	72 ± 6.2	31.7 ± 3.1	1.79 ± 0.09

3.2. Mechanical and dielectric properties

The mechanical properties of the sintered samples with different additive content were listed in Table 2. It can be seen from Table 2 that the bending strength, elastic modulus and fracture toughness appeared to have a linear growth and they significantly increase with the additive content from 18 MPa, 8.16 GPa and 1.12 MPa·m$^{1/2}$ to 72 MPa, 31.7 GPa and 1.79 MPa·m$^{1/2}$. The mechanical properties of the specimens were obviously quite sensitive to the additive content.

Figure 5 shows the influence of temperature and additive on the thermal diffusivity. The thermal diffusivity of the material decreased with the increase of temperature. It has been reported that the phase composition and porosity of the Si_2N_2O ceramics have important influence on the thermal diffusivity. When the sintering additive content was 2 wt.%, Si_2N_2O acted as the main crystalline phase. The thermal diffusivity of Si_2N_2O was lower than that of Si_3N_4, so the sample with 2 wt.% additive has the lowest thermal diffusivity. This result indicates that the Si_2N_2O ceramics has good thermal insulation properties and can meet the requirements of refractory properties for thermal insulation performance.

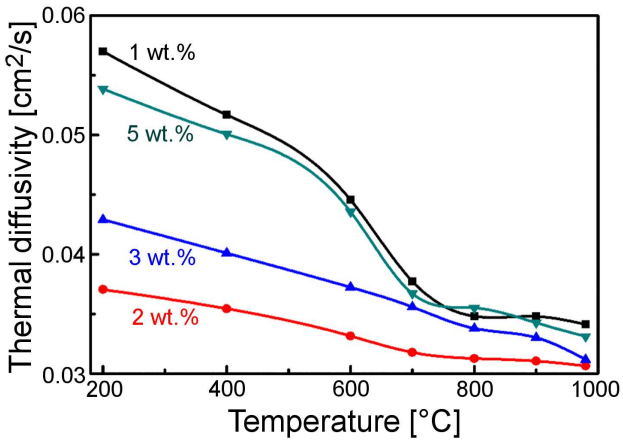

Figure 5. Thermal diffusivity of different samples as a function of temperature

It was reported that Si_2N_2O was unstable at high temperatures when exposed to oxidation atmosphere. It can be seen from Fig. 6 that the oxidation reaction of the Si_2N_2O causes weight increase. It is worth noticing that the initial oxidation rate of the porous Si_2N_2O ceramics was high and then the oxidation rate dropped rapidly with increase of the oxidation duration. The effects of the porosity on the oxidation resistance of the porous Si_3N_4 ceramics were described according to Porz and

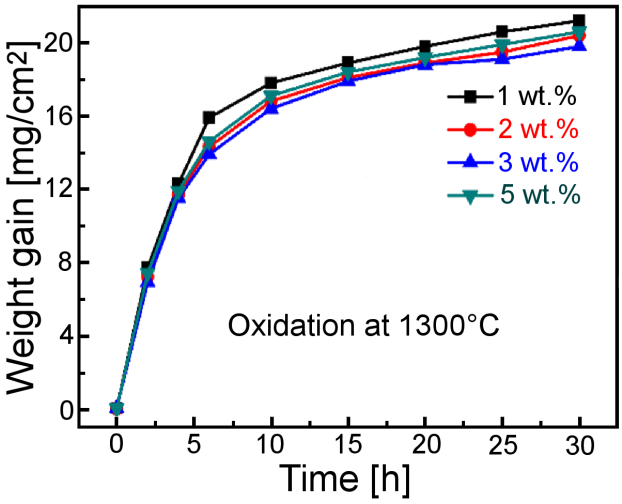

Figure 6. Weight gain of the different samples versus oxidation time at 1300 °C

Thümmler [38]. Figure 7 shows XRD patterns (A) and SEM images (B) of the surface of the different oxidized samples. According to the XRD pattern of the sample after oxidation, the formed oxidation product was recognized as SiO_2, which was expected according to Eq. 4. As can be seen from SEM images of the oxidized surfaces, very small particles just appeared on the surface of the sample with 1 wt.% sintering additive. However, the sample's surface was completely covered by glassy phase when the amount of sintering additive was more than 1 wt.%. The formed coherent SiO_2 layer blocked the oxygen diffusion to a certain degree, so further oxidation can be suppressed [24,39].

The thermal shock resistance performances of the samples were shown in Fig. 8. It can be seen that the residual strength showed little change from room temperature to 900 °C. The residual strength dropped sharply when the quenching temperature was above 1100 °C. However, for the sample with 2 wt.% sintering additive, its residual strength ratio was more than 70%, even though the quenching temperature was above 1300 °C. This result indicates that the porous Si_2N_2O ceramics prepared with 2 wt.% of sintering additive has excellent thermal shock resistance. These were caused by the difference of the thermal expansion coefficient between Si_2N_2O and oxidized layer (SiO_2) during cooling procedure. Therefore, the different thermal shock resistance of the samples could be attributed to the sintering additive and oxidation degree [40–42].

Apart from mechanical properties and high temperature properties, dielectric properties were also important

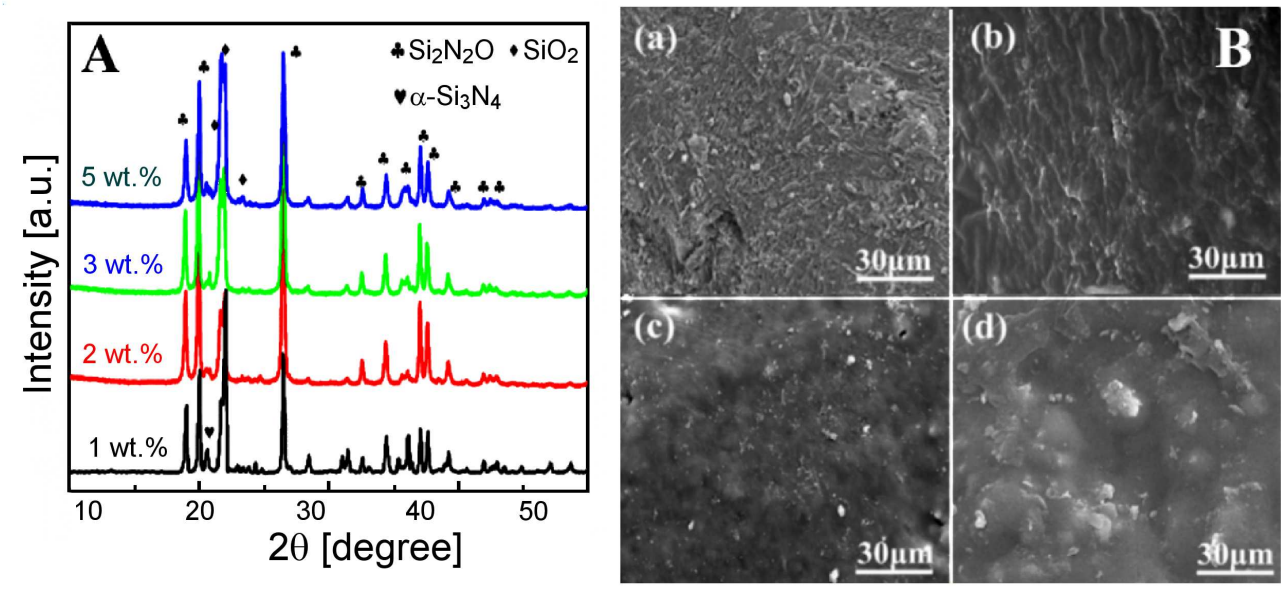

Figure 7. XRD patterns (A) and SEM images (B) of the surface of the different samples oxidized at 1300 °C for 30 h: a) 1, b) 2, c) 3 and d) 5 wt.%

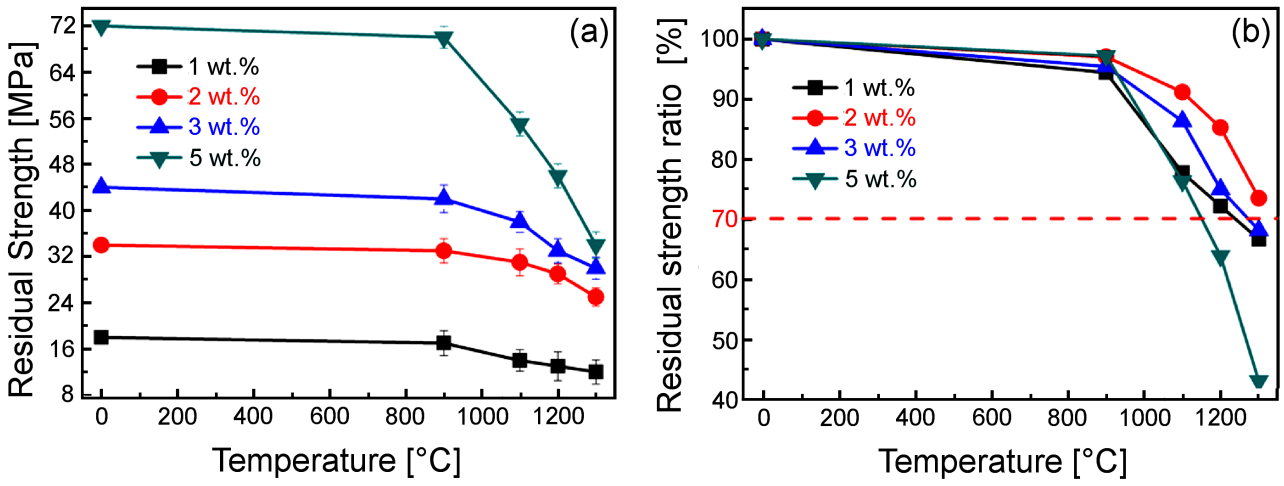

Figure 8. Residual strength and residual strength ratio of the Si_2N_2O ceramics with different Li_2O contents as a function of quenching temperature difference

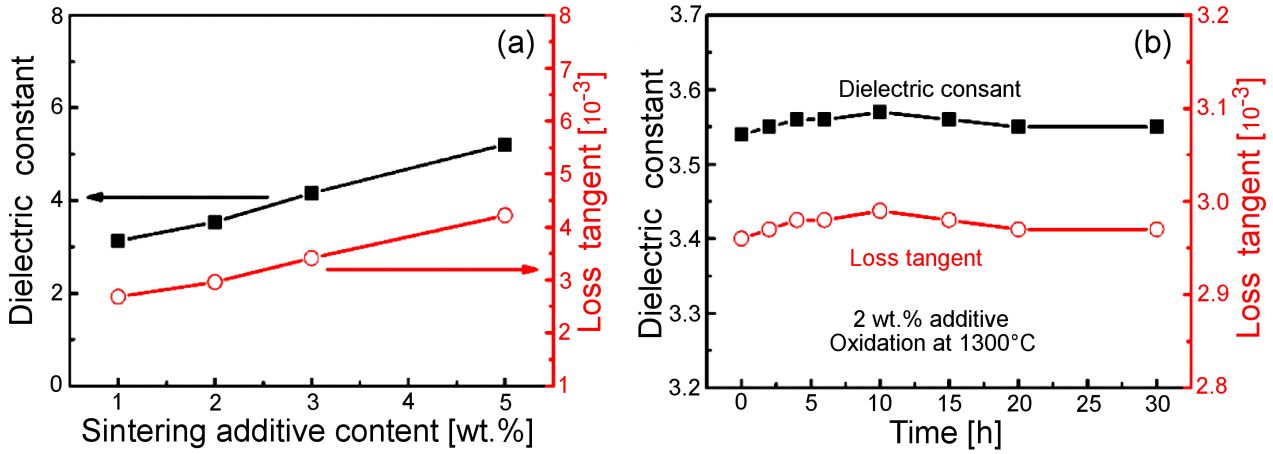

Figure 9. Effects of additive content (a) and oxidation time (b) on the dielectric constant and loss tangent of porous Si_2N_2O ceramics at 2.45 GHz

parameters for wave-transparent applications. Figures 9a and 9b showed the dielectric constant (ε) and loss tangent ($\tan\delta$) of the samples with different sintering additive content and oxidation time respectively, which were measured at the frequency of microwave sintering around 2.45 GHz. It can be found that all the samples exhibited reasonably ultra-low dielectric constant (ε = 3.13–5.12) and loss tangent ($\tan\delta$ = 0.00268–0.00422) with the increase of sintering additives. In addition, the dielectric constant was stable with the increase of oxidation time. So, the porous Si_2N_2O ceramics was suitable for microwave sintering furnace.

There were two factors affecting the dielectric constant of the samples [43]. Porosity was the main reason that was consistent with the Lichtenecker logarithmic equation [9,44] and empirical relation: the dielectric constant increased with the decrease of porosity. Another reason influencing the dielectric constant was the difference in composition, including different Si_3N_4 and Si_2N_2O content in the final composition and different sintering additive content in starting material. It has been discovered that residual Li^+ content was lower than 1/15 of the starting material because of the easy volatilization of Li_2O above 1300 °C [32,34,45]. On the other hand, the increasing amount of Si_3N_4 and SiO_2 caused by Si_2N_2O decomposition would increase dielectric constant. However, the content of those phases was also low. Therefore, the effect of sintering additive content and other phase on dielectric constant can be ignored, and porosity was considered to be the major factor influencing the dielectric constant. As for oxidation time, there are two aspects of changes happening in the products, namely the decrease of porosity and the rise of SiO_2 phase content as discussed above. Although the porosity decreased evidently after the oxidation, the oxidation products of Si_2N_2O can reduce the dielectric constant greatly. Because the dielectric constant of SiO_2 is lower than Si_2N_2O [14], the dielectric constant of Si_2N_2O ceramics was stable overall.

IV. Conclusions

Porous Si_2N_2O wave-transparent ceramics were prepared using Li_2CO_3 additive and vacuum sintering. The phase composition, microstructure, mechanical and dielectric properties can be tailored via directly adjusting the Li_2CO_3 amount. It was found that the generated Si_2N_2O became the main phase when the additive content was above 1 wt.%. The room temperature mechanical properties increased with the increase of additive content. The oxidation resistance and the thermal shock resistance were better when the additive content was 2 wt.%. The highest critical temperature difference (ΔT_c) could reach 1300 °C (residual strength ratio >70%). Furthermore, the dielectric properties were excellent (ε = 3.13–5.12, $\tan\delta$ = 0.00268–0.00422), which can be attributed to the porosity, Si_2N_2O phase and formed SiO_2 by oxidation. In conclusion, the porous Si_2N_2O ceramics with good mechanical properties and low dielectric properties have excellent potential for application in microwave sintering furnace.

Acknowledgement: This work was supported by the National Natural Science Foundation of China [51602287, 51932008 and 51772277]; Natural Science Research Project of Henan Educational Committee [17A430006]. National Key R&D Program of China (2017YFB0304000). The authors would like to thank for the support.

References

1. Y. Chen, B. Fan, B. Yang, W. Ma, G. Liu, H. Li, "Microwave sintering and fracture behavior of zirconia ceramics", *Ceram. Int.*, **45** [14] (2019) 17675–17680.
2. W. Li, B. Dai, K. Guan, R. Zhang, H. Li, "Preparation of mullite whiskers reinforced SiC/Al_2O_3 composites by microwave sintering", *Process. Appl. Ceram.*, **10** [4] (2016) 243–248.
3. Y. Chen, B. Fan, G. Shao, R. Zhang, "Preparation of large size ZTA ceramics with eccentric circle shape by microwave sintering", *J. Adv. Ceram.*, **5** (2016) 291–297.
4. S. Wei, L. Guan, B. Song, B. Fan, B. Zhao, R. Zhang, "Seeds-induced synthesis of SiC by microwave heating", *Ceram. Int.*, **45** [8] (2019) 9771–9775.
5. K. Kogut, K. Kasprzyk, B. Zboromirska-Wnukiewicz, T. Ruziewicz, "The research of ceramic materials for applications in the glass industry including microwave heating techniques", *IOP Conference Series Mater. Sci. Eng.*, **113** (2016) 012014–012022.
6. I. Ganesh, G. Sundararajan, "Hydrolysis-induced aqueous gelcasting of β-SiAlON-SiO_2 ceramic composites: The effect of AlN additive", *J. Am. Ceram. Soc.*, **93** [10] (2010) 3180–3189.
7. D.K. Kim, H. Neul Kim, Y. Hoon Seong, S. Soo Baek, E. Son Kang, Y. Gi Baek, "Dielectric properties of SiAlON ceramics", *Key Eng. Mater.*, **403** (2009) 125–128.
8. B. Li, K. Liu, C.-R. Zhang, S.-Q. Wang, "Fabrication and properties of borazine derived boron nitride bonded porous silicon aluminum oxynitride wave-transparent composite", *J. Eur. Ceram. Soc.*, **34** [15] (2014) 3591–3595.
9. X. Yang, B. Li, C. Zhang, S. Wang, K. Liu, C. Zou, "Fabrication and properties of porous silicon nitride wave-transparent ceramics via gel-casting and pressureless sintering", *Mater. Sci. Eng. A*, **663** (2016) 174–180.
10. Y. Cai, X. Li, J. Dong, "Properties of porous Si_3N_4 ceramic electromagnetic wave transparent materials prepared by technique combining freeze drying and oxidation sintering", *J. Mater. Sci. Mater. Electron.*, **25** [4] (2014) 1949–1954.
11. M.H. Bocanegra-Bernal, B. Matovic, "Mechanical properties of silicon nitride-based ceramics and its use in structural applications at high temperatures", *Mater. Sci. Eng. A*, **527** [6] (2010) 1314–1338.
12. T. He, "Effects of impurities on silicon dioxide dielectric properties", *Adv. Mater. Res.*, **1022** (2014) 56–59.
13. Q. Li, Z. Yang, Y. Miao, B. Liang, D. Cai, S. Wang, X. Duan, D. Jia, Y. Zhou, "Effect of the BN content on the thermal shock resistance and properties of BN/SiO_2 composites fabricated from mechanically alloyed SiBON powders", *RSC Advances*, **7** [77] (2017) 48994–49003.

14. S. Lin, F. Ye, J. Ding, C. Yang, J. Ma, S. Dong, Q. Liu, "Effects of pore diameters on phase, oxidation resistance, and thermal shock resistance of the porous Si_2N_2O ceramics", *J. Am. Ceram. Soc.*, **100** [5] (2017) 2190–2198.
15. X.-Y. Zhang, N. Li, T. Lan, Y.-J. Lu, K. Gan, J.-M. Wu, W.-L. Huo, J. Xu, J.-L. Yang, "In-situ reaction synthesis of porous Si_2N_2O-Si_3N_4 multiphase ceramics with low dielectric constant via silica poly-hollow microspheres", *Ceram. Int.*, **43** [5] (2017) 4235–4240.
16. J. Wen, H. Wang, L. Fan, L. Wei, M. Niu, H. Gao, Z. Cai, "Influences of rare-earth oxide additives on the formation and properties of porous Si_2N_2O ceramic", *J. Am. Ceram. Soc.*, **102** [1] (2019) 136–143.
17. L. Li, L. Gu, W. Yuan, J. Zhang, "Effect of magnesium titanate content on microstructures, mechanical performances and dielectric properties of Si_3N_4-based composite ceramics", *Ceram. Int.*, **43** [13] (2017) 9906–9911.
18. L. Gu, W. Yuan, R. Liao, H. Wang, B. Zhu, "Effect of TiO_2 addition on the microstructures, mechanical and dielectric properties of porous Si_3N_4-based ceramics", *Adv. Appl. Ceram. Struct. Funct. Bioceram.*, **116** [6] (2017) 348–354.
19. Y. Feng, H. Gong, Y. Zhang, X. Wang, S. Che, Y. Zhao, X. Guo, "Effect of BN content on the mechanical and dielectric properties of porous BNp/Si_3N_4 ceramics", *Ceram. Int.*, **42** [1] (2016) 661–665.
20. I. Sekercioglu, R.R. Wills, "Effect of Si_3N_4 powder reactivity on the preparation of the Si_2N_2O-Al_2O_3 silicon aluminum oxynitride solid solution", *J. Am. Ceram. Soc.*, **62** [11-12] (1979) 590–593.
21. Q. Tong, J. Wang, Z. Li, Y. Zhou, "Low-temperature synthesis/densification and properties of Si_2N_2O prepared with Li_2O additive", *J. Eur. Ceram. Soc.*, **27** [16] (2007) 4767–4772.
22. Z.-L. Lv, H.-L. Cui, H. Wang, X.-H. Li, G.-F. Ji, "Vibrational and dielectric properties and ideal strength of Si_2N_2O ceramic from first principles", *Ceram. Int.*, **43** [13] (2017) 10006–10012.
23. S. Wu, X. Li, "In-situ reactive synthesis of Si_2N_2O ceramics and its properties", *Metal. Mater. Trans. A*, **43** [12] (2012) 4859–4865.
24. S. Lin, Y. Feng, S. Dong, M. Jie, B. Zhang, J. Ding, "Mechanical, dielectric properties and thermal shock resistance of porous silicon oxynitride ceramics by gas pressure sintering", *Mater. Sci. Eng. A*, **635** (2015) 1–5.
25. L. ShuQin, P. YuChen, Y. ChangQing, L. JiaLu, "Mechanical and dielectric properties of porous Si_2N_2O-Si_3N_4 in situ composites", *Ceram. Int.*, **35** [5] (2009) 1851–1854
26. Q. Tong, Y. Zhou, J. Zhang, J. Wang, M. Li, Z. Li, "Preparation and properties of machinable Si_2N_2O/BN composites", *Int. J. Appl. Ceram. Technol.*, **5** [3] (2008) 295–304.
27. X. Dong, J. Liu, H. Du, A. Guo, M. Liu, "Microstructure characterization of in situ synthesized porous Si_2N_2O ceramics using spodumene additive", *Ceram. Int.*, **39** [4] (2013) 4657–4662.
28. X. Yang, B. Li, C. Zhang, S. Wang, K. Liu, C. Zou, "Design and fabrication of porous Si_3N_4-Si_2N_2O in situ composite ceramics with improved toughness", *Mater. Design*, **110** (2016) 375–381.
29. S. Wang, Z. Yang, X. Duan, D. Jia, F. Ma, B. Sun, Y. Zhou, "Fabrication and characterization of in situ porous Si_3N_4-Si_2N_2O-BN ceramic", *Int. J. Appl. Ceram. Technol.*, **11** [5] (2014) 832–838.
30. Y. Shao, D. Jia, Y. Zhou, B. Liu, "Novel method for fabrication of silicon nitride/silicon oxynitride composite ceramic foams using fly ash cenosphere as a pore-forming agent", *J. Am. Ceram. Soc.*, **91** [11] (2008) 3781–3785.
31. H. Cheng, Y. Li, E. Kroke, S. Herkenhoff, "In situ synthesis of Si_2N_2O/Si_3N_4 composite ceramics using polysilyloxycarbodiimide precursors", *J. Eur. Ceram. Soc.*, **33** [11] (2013) 2181–2189.
32. L. Fan, M. Zhou, H. Wang, Z. Shi, X. Lu, C. Wang, "Low-temperature preparation of β-Si_3N_4 porous ceramics with a small amount of Li_2O-Y_2O_3", *J. Am. Ceram. Soc.*, **97** [5] (2014) 1371–1374.
33. Z. Tatli, D.P. Thompson, "Low temperature densification of silicon nitride using Li_2O-based surface coatings", *Ceram. Int.*, **38** [1] (2012) 15–21.
34. B. Matovic, G. Rixecker, F. Aldinger, "Pressureless sintering of silicon nitride with lithia and yttria", *J. Eur. Ceram. Soc.*, **24** [12] (2004) 3395–3398.
35. L. Yu, J. Zhao, X. Yan Yue, J. Yang Li, H. Ru, "Microstructure and properties of graphite embedded SiC composite by coating method", *Adv. Mater. Res.*, **105** (2010) 855–858.
36. F.H. Chung, "Quantitative interpretation of X-ray diffraction patterns of mixtures. II. Adiabatic principle of X-ray diffraction analysis of mixtures", *J. Appl. Crystall.*, **7** [6] (1974) 526–531.
37. X. Zhou, D. Liu, H. Bu, L. Deng, H. Liu, P. Yuan, P. Du, H. Song, "XRD-based quantitative analysis of clay minerals using reference intensity ratios, mineral intensity factors, Rietveld, and full pattern summation methods: A critical review", *Solid Earth Sci.*, **3** [1] (2018) 16–29.
38. F. Porz, F. Thümmler, "Oxidation mechanism of porous silicon nitride", *J. Mater. Sci.*, **19** [4] (1984) 1283–1295.
39. J. Persson, P.-O. Käll, M. Nygren, "Interpretation of the parabolic and nonparabolic oxidation behavior of silicon oxynitride", *J. Am. Ceram. Soc.*, **75** [12] (1992) 3377–3384.
40. K. Houjou, K. Ando, M.C. Chu, S.P. Liu, S. Sato, "Effect of sintering additives on the oxidation behavior of Si_3N_4 ceramics at 1300 °C", *J. Eur. Ceram. Soc.*, **25** [5] (2005) 559–567.
41. J. She, J.-F. Yang, D.D. Jayaseelan, N. Kondo, T. Ohji, S. Kanzaki, Y. Inagaki, "Thermal shock behavior of isotropic and anisotropic porous silicon nitride", *J. Am. Ceram. Soc.*, **86** [4] (2003) 738–740.
42. F. Ye, L. Liu, H. Zhang, B. Wen, "Thermal shock behavior of 30 wt%BAS/Si_3N_4 self-reinforced composite", *J. Alloys Compds.*, **493** [1] (2010) 272–275.
43. D. Jia, Y. Shao, B. Liu, Y. Zhou, "Characterization of porous silicon nitride/silicon oxynitride composite ceramics produced by sol infiltration", *Mater. Chem. Phys.*, **124** [1] (2010) 97–101.
44. A.V. Goncharenko, V.Z. Lozovski, E.F. Venger, "Lichtenecker's equation: applicability and limitations", *Optics Commun.*, **174** [1] (2000) 19–32.
45. B. Matovic, G. Rixecker, F. Aldinger, "Densification of Si_3N_4 with $LiYO_2$ additive", *J. Am. Ceram. Soc.*, **87** [4] (2004) 546–549.